



Cracow University of Technology
Department of Electrical and Computer Engineering
Institute of Electromechanical Energy Conversion, E-2



“Simulink models of faulty induction machines for drives applications”

SUMMARY OF DOCTORAL DISSERTATION

BY

Alejandro Fernández Gómez, M.Sc.

Supervisor: ***Dr. Hab. Konrad Weinreb***

Kraków 2015

Chapter 1 PhD Thesis Brief

1.1 Objectives

The aim of the research is to develop mathematical model of squirrel cage induction motors and to create dynamic models in Matlab/Simulink ready to be implemented in drive applications. Following the classical model of IM, faulty models can also be reduced to a system of four electrical equation, two equations either for stator and rotor currents, and two mechanical equations. The use of models with a reduce number of equations will reduce the simulation time (Despite of the fact that technology is improving incredible fast the time require to run a simulation is still an important constrain to be taken into consideration).

Mathematical models of squirrel cage induction motor have been simplified considering tree phase rotor windings as the configuration of a slip-ring induction motor. The rotor bar currents are not accessible, the diagnosis of the fault is mainly conducted by studying the stator phase currents in different reference frames applying Motor Current Signature Analysis techniques. Therefore, the rotor currents are not being subject to any analysis. Theoretically, the effects of the rotor quantities and the physical phenomena inside the rotor cause the same effect over the stator phase currents in both configurations of the induction motor.

The simplification is as follows: in case of considering the squirrel cage rotor the number of rotor currents to be defined is equal to the number of bars plus one extra current which represent the current flowing through one of the rings. The magneto-motive force (MMF) in each of the mesh is also approximated by a sinusoidal function with small amplitude due to the fact that it depends on the angle between bars $\gamma = 2 * \pi / N$. Instead to considering each independent mesh current the bars have been grouped in three sets and only one mesh current has been considered. The sum of all MMFs along the rotor bars in both cases will be equivalent leading to the same effects over the stator phase currents.

The objectives are listed below:

- Develop a Matlab/Simulink Library of faulty dynamic induction motor models for diagnosis purposes
- Design a test-bench and a data acquisition system
- Validation of simulation results with experimental data
- Apply advance signal processing techniques to the data stored
- Explore the suitability of these models for diagnosis of faults

In the market there are many software tools which offer friendly user interfaces and tools for modelling electrical systems. However, Matlab/Simulink has been chosen due to the fact that offers the possibility of C and Hardware Description Language (HDL) code generation and the compatibility it has with many industrial solutions.

The most important outcome of the research is to have a library of exchangeable models to investigate new control laws that improve the ability of drives to control the induction motor. In the course of the thesis, it will be proved, that despite the assumptions made, the models are suitable for studying the behavior of a fault by means of MCSA techniques, widely used by the scientific community, supported by experimental results.

1.2 Cele

Celem badań jest opracowanie modeli matematycznych silników indukcyjnych klatkowych i stworzenie modeli dynamicznych z użyciem oprogramowania Matlab/Simulink, gotowych do stosowania w aplikacjach napędowych. Zgodnie z klasycznym modelem silnika indukcyjnego, modele silnika z wadą również mogą być sprowadzone do układu czterech równań: dwóch równań napięć stojana lub wirnika oraz dwóch równań mechanicznych. Zastosowanie modeli ze zmniejszoną liczbą równań zmniejsza również czas potrzebny na symulacje (pomimo bardzo szybkiego rozwoju i ciągłego ulepszania technologii, czas wymagany do przeprowadzenia symulacji wciąż stanowi ważne ograniczenie, które musi zostać wzięte pod uwagę).

Modele matematyczne klatkowego silnika indukcyjnego zostały uproszczone przez przyjęcie trójfazowego uzwojenia wirnika, jak w silniku pierścieniowym. Prądy w prętach wirnika nie są dostępne, a diagnoza uszkodzenia jest przeprowadzana głównie poprzez badanie prądów fazowych stojana w różnych układach odniesienia z zastosowaniem techniki MCSA. Dlatego też prądy wirnika nie są poddane żadnej analizie.

Teoretycznie, wpływ właściwości wirnika oraz zjawisk fizycznych zachodzących w jego wnętrzu na fazowe prądy stojana jest taki sam w obydwu konfiguracjach silnika indukcyjnego.

Uproszczenie prowadzi do następującego spostrzeżenia: w przypadku silnika klatkowego liczba zdefiniowanych prądów wirnika jest równa liczbie prętów, plus dodatkowo prąd, który reprezentuje prąd przepływający przez jeden z pierścieni zwierających.

Siła magnetomotoryczna (MMF) w każdym z oczek klatki jest również aproksymowana funkcją sinusoidalną o małej amplitudzie ze względu na fakt, iż zależy ona od kąta nachylenia pomiędzy prętami $\gamma = 2\pi/N$. Zamiast rozważać prąd pojedynczego oczka, pręty zostały zebrane w trzy grupy, reprezentowane przez tylko jeden prąd oczkowy w grupie. Suma wszystkich sił magnetomotorycznych wzdłuż prętów wirnika w obu przypadkach będzie równa, co ma taki sam wpływ na fazowe prądy stojana.

Poniżej wymienione są cele badawcze:

- stworzenie biblioteki modeli dynamicznych uszkodzonych silników indukcyjnych za pomocą oprogramowania Matlab/Simulink dla celów diagnostycznych
- zaprojektowanie stanowiska pomiarowego i systemu zbierania danych
- walidacja wyników symulacji z użyciem danych doświadczalnych
- zastosowanie zaawansowanych technik przetwarzania sygnałów na przechowywanych danych
- zbadanie adekwatności opracowanych modeli do celów diagnostycznych

Na rynku znajduje się wiele narzędzi oprogramowania, które oferują przyjazne użytkownikowi interfejsy i narzędzia modelowania systemów elektrycznych. Niemniej jednak, dla celów tej pracy badawczej wybrano narzędzie Matlab/Simulink, jako że oferuje możliwość generacji kodu C i HDL (Hardware Description Language) oraz ze względu jego kompatybilność, z wieloma rozwiązaniami stosowanymi w przemyśle (w rozdziale drugim przedstawione zostaną zalety wyboru programu Matlab/Simulink).

Najważniejszym wynikiem pracy badawczej jest stworzenie biblioteki wymiennych modeli w celu zbadania nowych przepisów kontrolnych, które poprawiają zdolność napędów do kontroli silników indukcyjnych. W ramach poniższej pracy zostanie udowodnione, że pomimo poczynionych założeń, modele te nadają się do,

Summary “Simulink models of faulty induction machines for drives applications”

wspieranego przez wyniki doświadczalne, badania specyfiki danego uszkodzenia za pomocą technik MCSA, powszechnie stosowanych przez środowiska naukowe.

1.3 Chapter Summary

The thesis has been structured as follows:

- Chapter 2 – State of Art: the common faults in IM will be described as well as the main signal processing techniques. A review of the main contributions in the field of induction motor fault diagnosis and the suitability of Matlab for modelling electromechanical systems are also discussed.
- Chapter 3 – Modelling electrical machines under fault condition: dynamic faulty machine models have been developed following the winding function approach. The chapter will guide the lector through the mathematical procedure. An explanation of the physical phenomena occurring inside the machine for each fault will be described from the point of view of mathematics.
- Chapter 4 – Harmonic Balance Method: it is a method of steady-state analysis for electrical machine equations with periodic coefficients which consists of a linear system of algebraic equations. The method takes into consideration the physical phenomena inside the machine when it is affected by a fault and their effects on the harmonic content of the stator currents. It is equivalent to the symbolic calculus for electric circuits.
- Chapter 5 – Test Bench Set-up: it includes a description of the lab equipment used and the estimation of the IM parameters.
- Chapter 6 – Matlab-Simulink Implementation of Dynamic IM Models: the Simulink model performance is analyzed supported by simulation results.
- Chapter 7 – Matlab Implementation of Steady State IM Models: the Matlab model performance is analyzed supported by simulation results.
- Chapter 8 – Experimental Results - Validation of Simulation Results: discussion about the simulation results for different operation points of the induction motor validated by experimental data of dynamic and steady state models.
- Chapter 9 – Drives Applications with Faulty Induction Motor models: Implementation into a Zynq all programmable System on a Chip (SoC) (ARM+FPGA): practical case of model implementation. It shows the results of the work carried out at ABB Corporate Research Center Poland as part of the task planned within the Energy Smartops project.
- Chapter 10 – Analysis and Diagnosis of Electrical and Mechanical Faults in Induction Motors: it contains a summary of the research work published by the author of the thesis in the field of fault diagnosis of induction motors.
- Chapter 11 – Conclusions

Chapter 2 State of Art

The main techniques used to diagnose fault on electrical machines has been discussed. Some of them are mentioned below:

Summary “Simulink models of faulty induction machines for drives applications”

1. Stator Faults: the common techniques used to diagnose faults in stator are [10]:
 - a. Magnetic Flux: a measure of the axial flux can reveal distortion of the air-gap flux or comparing the voltages across different stator coils.
 - b. Rotor speed: studying the magnitude variations of the 100 Hz frequency component.
 - c. Temperature: degradation of the insulation material cause increased in losses. A detection of hot spots in the stator core is used to detect such problems [15].
 - d. Stator currents: as it has been shown in table III the stator defects add frequency components to the stator currents [19].
2. Rotor Faults – Broken bar detection: Detection of BBs typically performed studying the low-frequency sidebands around the main component, i. e., the relation of the sideband magnitudes as fault indicator, is not always effective [9]. High frequency components around the 3th, 4th, 5th, 7th and PSH harmonics can be useful [1] [5] [12] [16]. The FFT is the basic analysis but it has some disadvantages such as the need of knowing the motor speed, the confusion with mechanical fault or spectra leakage. In such situations, WT or HT are a good solution to overcome those disadvantages [18]. In the following section some of the research work done in this area is summarized.
3. Rotor Faults – Eccentricity detections: The difficulty in detecting types of eccentricities stems from the fact that SE and DE usually appear simultaneously. Both types of eccentricities add similar additional frequencies making it difficult to tell the difference between them. Moreover, not all frequency components will appear in each motor (they depend on the number of rotor bars). Another difficulty is that those frequencies can appear due to other fault types. Several models have been proposed in literature [2] [3] [4] [6] [8] [11] [17] including all or main harmonics. For instance, each author had a particular way of calculating the geometrical length of the air-gap in order to approximate the value of the permeance function to the real one accounting for stator/rotor slots, saturation or simply the Carter coefficient. Many of the analysis conducted in this field are based in the comparison of the low/high frequency magnitudes well known in literature establishing different indexes with the aim of either distinguish faults or detecting the severity level.

Finally, the suitability of MATLAB/SIMULINK as simulation software is also discussed:

Nowadays MATLAB/SIMULINK offers an integrated environment to simulate the transient and steady state of electrical machines with time-varying variables under different conditions which allow the simulation of a large number of operation modes. An important advantage of that package is the waveform representation of electrical signals. The simple fact of knowing the equations is not enough to obtain results successfully. This software requires a hard effort in understanding the procedure of resolution of differential equations.

In this Thesis, MATLAB/SIMULINK has been used to create a toolbox of Faulty Induction Motor models for analysis and fault diagnosis purposes due to the fact that it is a software with extensive use in the teaching and engineering field. It provides many toolboxes related to signal processing techniques, Digital Signal Processor (DSP) programming and it offers compatibility with DAQ devices from many manufactures. Moreover it allows creating and customizing user interfaces for easy visualization of model results and/or organization of simulation

Summary “Simulink models of faulty induction machines for drives applications”

options for non-expert programmer users. Many publications have shown Simulink models for implementation of IM [7] [13] [14] [17]; nevertheless, only the healthy machine has been studied.

Chapter 3 Modelling Electrical Machines under Fault Condition

This chapter explains the methodology followed to develop dynamic induction motor models under fault condition: Lagrange function and Winding Function Approach (WFA). The different physical phenomena that occur inside the machine when it is affected by faults are analyzed by mathematical equations leading to models with different levels of complexity. These models can be reduced to two sets of electrical and mechanical equations following the classical model of IM by applying specific transformation matrices widely known by the scientific community with the exception of the Mixed Eccentricity (ME) model.

3.1 Lagrange Equation and Winding Function Approach

The interaction of the stator and rotor magnetic fields is the fundamental mechanism by which the electrical energy is converted into mechanical energy and vice versa in IMs. Since failures produces a distortion of the magnetic fields it may seem logic to develop algorithms which describes the distribution of the magnetic field in the machine an use software based on FEM to detect faults in IMs. Nevertheless, this type of analysis requires solving Laplace and Poisson’s equations which is a time consuming process. As fault diagnosis of IMs is mainly based on the study of the harmonic content of currents, fluxes torque and/or speed, the development of models based on groups of magnetic circuits’ couple each other, provides a better alternative to understand the physical phenomena associated with failures and the fault consequences in the IM’s variables. Those electromagnetic circuits are composed by a set of resistance and inductance matrices.

Electromechanical converters such as induction motors can be mathematically described by Hamilton’s and Lagrange’s functions but in practice only Lagrange equation is used as Hamilton’s development is much more complicated.

Assuming the linearity of the magnetic circuit, the converter equations following the Lagrange’s functions are as follows:

$$\frac{d}{dt}(\mathbf{L}(\varphi) \cdot \mathbf{i}) + \mathbf{R} \cdot \mathbf{i} = \mathbf{u} \quad (3.1)$$

$$J \frac{d^2\varphi}{dt^2} + D \frac{d\varphi}{dt} = \frac{1}{2} \cdot \mathbf{i}^T \cdot \frac{\mathbf{L}(\varphi)}{\partial\varphi} \cdot \mathbf{i} + T_m \quad (3.2)$$

Winding Function Approach (WFA) is a method for estimation of the machine inductances and for the geometry definition of the air-gap. The inductances values are calculated as function of the linked flux along the air-gap of the machine, which is defined by so-called permeance function. This method has some limitation due to the fact that following assumptions have to be taken:

- Linear magnetic field
- The magnetic material has infinite permeance
- Fluxes crossed the air-gap radially
- Eddy and Hysteresis currents are neglected

Summary “Simulink models of faulty induction machines for drives applications”

In addition it has been assumed that saturation and slotting effects are also neglected.

In order to obtain the magnetic field distribution is needed to define the MMF function of all windings. The MMF is quasi periodic, hence, it can be represented by Fourier series. For distributed coils in stator the general form used for the MMF function is:

$$\theta(x, t) = i(t) \cdot \sum_{\rho=1}^{\infty} \frac{4}{\pi} \cdot \frac{w \cdot k_{\rho}}{2 \cdot \rho} \cdot \cos \rho(x - \alpha) \quad (3.3)$$

where “ $i(t)$ ” is the current flowing through the coil, “ k_{ρ} ” is the winding factor, “ w ” is number of winding turns, “ ρ ” the order of the harmonic and “ α ” is the angle between coils.

The permeance function depends on the magnetic circuit type and defines the geometry of the air-gap along the circumference. One important property of the permeance function is that is a periodic function. $\lambda(x, \varphi)$ is the inverse of the air-gap length:

$$\lambda(x, \varphi) = \frac{1}{\delta(x, \varphi)} \quad (3.4)$$

A new function is introduced: The Ampere-turn function $w(x, t)$ based on MMF function.

$$w(x, t) = \frac{1}{i(t)} \cdot \frac{d\theta(x, t)}{dx} = \sum_{\rho=1}^{\infty} \left(-\frac{2}{\pi}\right) w k_{\rho} \sin \rho(x - \alpha_{\rho}) \quad (3.5)$$

The final expression for linked flux of the winding “ n ” due to magnetic field forced by the winding “ k ” for “ ρ ” harmonic is as follows:

$$\Psi_{n,k} = r \cdot l \cdot \sum_{\rho=1}^{\infty} \left(\int_{\alpha_{n,\rho} - \frac{\pi}{\rho}}^{\alpha_{n,\rho}} \left(\sum_{m=1}^{\rho} \left(-\frac{2}{\pi}\right) w_n k_{n,\rho} \sin \rho(x - \alpha_{\rho}) \right) \cdot \int_{\alpha_{\rho,m}}^{\alpha_{k,m}} B_k(\zeta, \varphi, t) d\zeta \right) dx \quad (3.6)$$

Inductance values are obtained as,

$$L_{n,k} = \Psi_{n,k} / i_n \quad (3.7)$$

In addition, there is another type of inductance left: the Leakage inductance. In a real machine part of the linked flux do not cross the air-gap, for instance, those lines that encircle only the stator and rotor coils (bars).

The linked fluxes can be classified in:

- Stator and rotor slot leakage inductance
- Zig-zag leakage inductance
- Differential leakage inductance
- End connection leakage inductance
- Skewing leakage inductance

Generally, total leakage inductance is accounted as the 10% of the self-inductance.

It may happens that the machine inductance depends on the rotation angle “ φ ”. With the aim of simplified the calculations following transformation matrices are used to eliminate such dependence. As a result, the converter equations can be reduced to a system of differential equations with constant coefficient matrices. When applying these transformation matrices, the zero sequence of the symmetrical components can be neglected. If the steady state of the machine is considered, for a given speed, the converters equations are even reduced to a set of simply lineal equations by means of the Harmonic Balance Method (HBM) explained in next chapter.

Equation 3.1 and 3.2 can be expressed in matrix form:

$$\begin{bmatrix} U_s \\ U_r \end{bmatrix} = \begin{bmatrix} R_s & 0 \\ 0 & R_r \end{bmatrix} \cdot \begin{bmatrix} I_s \\ I_r \end{bmatrix} + \frac{d}{dt} \begin{bmatrix} L_{s,s}(\varphi) + L_s^\sigma & L_{s,r}(\varphi) \\ L_{r,s}(\varphi) & L_{r,r}(\varphi) + L_r^\sigma \end{bmatrix} \cdot \begin{bmatrix} I_s \\ I_r \end{bmatrix} \quad (3.8)$$

$$J \frac{d^2\varphi}{dt^2} + D \frac{d\varphi}{dt} = T_{elec} + T_m = \frac{1}{2} \cdot [(I_s)^T \quad (I_r)^T] \cdot \begin{bmatrix} L_{s,s}(\varphi) & L_{s,r}(\varphi) \\ L_{r,s}(\varphi) & L_{r,r}(\varphi) \end{bmatrix} \cdot \begin{bmatrix} I_s \\ I_r \end{bmatrix} + T_m \quad (3.9)$$

For all the dynamic models develop on the thesis, the inductances and resistances are changed according the fault. For instance, when it comes to model broken bars, R_r is substitute for and equivalent matrix, R_{eq} , that contains the asymmetry and symmetry coefficients, k_{as} & k_s , well known among the research community.

The following models with faults has been created: 1/ Cage Asymmetry; 2/ Static Eccentricity; 3/ Dynamic Eccentricity; 4/ Simulation of Mechanical faults.

Moreover, the electromagnetic torque, T_{elec} , will depend on the transformation matrices applied as well.

3.2 Examples of Final Induction motor Models Following the WFA

3.2.1 Modelling Induction motor Mechanical Faults: Eccentricities

The Eccentricity is inherited to the electrical machine. It occurs when the air-gap is not constant, which means, the distance between the inner-circumference of the stator and the outer circumference of the rotor is not constant. In fact that happens since the stator and rotor are built with slots to allocate the windings.

The permeance function “ λ ” is used to estimate the length of the air-gap linked fluxes along the circumference which crossed radially the stator and rotor. A simply approach based on how the air-gap is defined for other motor topologies can be used for modelling eccentricities.

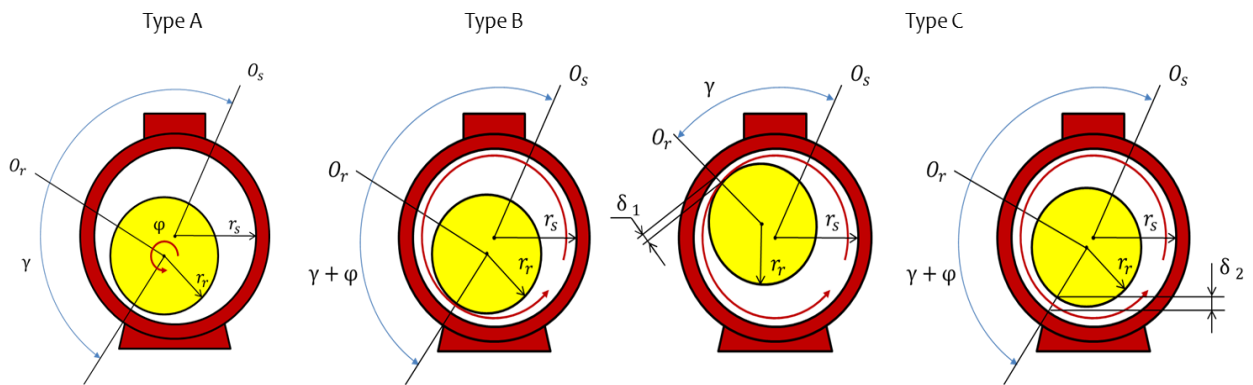


Fig. 3.1 Air-gap topology

Fig. 3.2 shows those topologies (All represent machines with salient poles on stator, rotor or both).

The position and length of the air-gap for SE is fixed in time and space which corresponds to type B. Consequently, the permeance function will depend on an arbitrary angle “ x ” respect to the stator reference axis. In case of DE, the length keeps constant but the position rotates corresponding to type A. Hence, the permeance function will depend on the rotational angle “ φ ”. Finally, for ME, both position and length change, so, the permeance function depends in both angles, “ x ” & “ φ ”. Moreover, as it is a periodic function, it can be defined by Fourier series.

Table I Permeance function types

Type	A	B	C
Permeance Function (Exponential series)	$\lambda(y) = \sum_{r=-\infty}^{\infty} A_r \cdot e^{j \cdot r \cdot y}$	$\lambda(x) = \sum_{r=-\infty}^{\infty} A_r \cdot e^{j \cdot r \cdot x}$	$\lambda(x, \varphi) = \sum_{r=-\infty}^{\infty} \sum_{s=-\infty}^{\infty} A_{r,s} \cdot e^{j \cdot r \cdot x} \cdot e^{j \cdot r \cdot \varphi}$
Permeance Function (Cos. series)	$\lambda(y) = A_0 + \sum_{r=1}^{\infty} A_r \cdot \cos r(y)$	$\lambda(x) = A_0 + \sum_{r=1}^{\infty} A_r \cdot \cos r(x)$	$\lambda(x, \varphi) = A_{0,0} + \sum_{r=1}^{\infty} \sum_{s=1}^{\infty} A_{r,s} \cdot \cos r(x) \cdot \cos s(\varphi)$

“ A ” are the Fourier coefficients and “ $y = x - \varphi$ ”.

Changes of the air-gap regarding eccentricities can be approximated by geometrical relationships between the machine symmetry axial axis “ O_s ” and the path described by the rotor centre “ O_r ”.

3.2.1.1 Mixed Eccentricity

Following the WFA, applying the above permeance function and considering only the effects of the main MMFs that contains p -harmonic (equation 3.3), the inductance matrices of an induction motor (equation 3.6) with ME in symmetrical components are:

- Self-Inductance Stator:

$$\begin{aligned}
 L_{s,s} = & \left(\sum_{m=0}^{\infty} L_1 A_{0,m} \cos(m\varphi') - \left[\sum_{m=0}^{\infty} L_1 A_{p,m} \cos(m\varphi') \cdot \frac{\sum_{m=0}^{\infty} A_{p,m} \cos(m\varphi')}{\sum_{m=0}^{\infty} A_{0,m} \cos(m\varphi')} \right] \right) \cdot \begin{bmatrix} 0 & 0 & 0 \\ 0 & \frac{3}{2} & 0 \\ 0 & 0 & \frac{3}{2} \end{bmatrix} + \\
 & + \left(\frac{1}{2} \sum_{m=0}^{\infty} L_1 A_{2p,m} \cos(m\varphi') - \left[\sum_{m=0}^{\infty} L_1 A_{p,m} \cos(m\varphi') \cdot \frac{\sum_{m=0}^{\infty} A_{p,m} \cos(m\varphi')}{\sum_{m=0}^{\infty} A_{0,m} \cos(m\varphi')} \right] \right) \cdot \begin{bmatrix} 0 & 0 & 0 \\ 0 & 0 & e^{j2p\varphi} \\ 0 & e^{-j2p\varphi} & 0 \end{bmatrix} + \\
 & + \begin{bmatrix} L_{\sigma s}^0 & 0 & 0 \\ 0 & L_{\sigma s}^1 & 0 \\ 0 & 0 & L_{\sigma s}^2 \end{bmatrix}; \text{ where } L_1 = r \cdot l \cdot \mu_0 \frac{4}{\pi} \left(\frac{w_s k_s}{p} \right)^2
 \end{aligned} \tag{3.8}$$

- Self-Inductance Rotor:

$$\begin{aligned}
 L_{r,r} = & \left(\sum_{m=0}^{\infty} L_2 A_{0,m} \cos(m\varphi') - \left[\sum_{m=0}^{\infty} L_2 A_{p,m} \cos(m\varphi') \cdot \frac{\sum_{m=0}^{\infty} A_{p,m} \cos(m\varphi')}{\sum_{m=0}^{\infty} A_{0,m} \cos(m\varphi')} \right] \right) \cdot \begin{bmatrix} 0 & 0 & 0 \\ 0 & \frac{3}{2} & 0 \\ 0 & 0 & \frac{3}{2} \end{bmatrix} + \\
 & + \left(\frac{1}{2} \sum_{m=0}^{\infty} L_2 A_{2p,m} \cos(m\varphi') - \left[\sum_{m=0}^{\infty} L_2 A_{p,m} \cos(m\varphi') \cdot \frac{\sum_{m=0}^{\infty} A_{p,m} \cos(m\varphi')}{\sum_{m=0}^{\infty} A_{0,m} \cos(m\varphi')} \right] \right) \cdot \begin{bmatrix} 0 & 0 & 0 \\ 0 & 0 & e^{j2p\varphi} \cdot e^{-j2p\varphi} \\ 0 & e^{-j2p\varphi} \cdot e^{j2p\varphi} & 0 \end{bmatrix} + \\
 & + \begin{bmatrix} L_{\sigma r}^0 & 0 & 0 \\ 0 & L_{\sigma r}^1 & 0 \\ 0 & 0 & L_{\sigma r}^2 \end{bmatrix}; \text{ where } L_2 = r \cdot l \cdot \mu_0 \frac{4}{\pi} \left(\frac{w_r k_r}{p} \right)^2
 \end{aligned} \tag{3.9}$$

- Mutual Inductance

$$M_{sr} = \left(\frac{3}{2} \right) \cdot \left(\sum_{m=0}^{\infty} L_3 A_{0,m} \cos(m\varphi') - \left[\sum_{m=0}^{\infty} L_3 A_{p,m} \cos(m\varphi') \cdot \frac{\sum_{m=0}^{\infty} A_{p,m} \cos(m\varphi')}{\sum_{m=0}^{\infty} A_{0,m} \cos(m\varphi')} \right] \right) \cdot \begin{bmatrix} 0 & 0 & 0 \\ 0 & e^{jp\varphi} & 0 \\ 0 & 0 & e^{-jp\varphi} \end{bmatrix} +$$

$$+ \left(\frac{1}{2} \sum_{m=0}^{\infty} L_3 \Lambda_{2p,m} \cos(m\varphi') - \left[\sum_{m=0}^{\infty} L_3 \Lambda_{p,m} \cos(m\varphi') \cdot \frac{\sum_{m=0}^{\infty} \Lambda_{p,m} \cos(m\varphi')}{\sum_{m=0}^{\infty} \Lambda_{0,m} \cos(m\varphi')} \right] \right) \cdot \frac{3}{2} \cdot \begin{bmatrix} 0 & 0 & 0 \\ 0 & 0 & e^{-jv\varphi+j2p\gamma} \\ 0 & e^{jv\varphi-j2p\gamma} & 0 \end{bmatrix} +$$

where $L_3 = r \cdot l \cdot \mu_0 \frac{1}{\pi} \cdot \left(\frac{w_s k_s}{p} \right) \left(\frac{w_r k_r}{p} \right)$

(3.10)

Chapter 4 Harmonic Balance Method

In the previous chapter it has been shown that the converter’s equations can be reduced to two sets of four electrical and two mechanical linear differential equations with constant coefficients periodic matrices. Classical method based on circuit theory can easily solve the system in analytical form. Furthermore, if the steady state of the machine is considered, which means that the solution of the mechanical equation is known, the system can be reduced to linear equations.

A method for steady state analysis of electrical machines with non-linear differential equations with periodic coefficient is presented for those cases in which the transformation matrix does not obtain matrices with constant coefficients: “Harmonic Balance Method” (HBM). This methodology has been applied to determine the steady state of an induction motor affected by ME. Additionally, models for SE and DE has also been created to compare with dynamic models obtained from WFA. They have accounted the main MMFs and the presence of air-gap asymmetry which cause the appearance of additional harmonics of magnetic permeance assuming linear magnetic circuit, three symmetrical stator and rotor windings, “p” pair of poles and there phase rotor mesh currents. Moreover, the same assumptions made in order to obtain a dynamic model of IM are also assumed.

Model of all the eccentricities are listed below, where:

- Ω_o and Ω are the angular velocity of the net and rotor
- \mathbf{E} is the identity matrix
- $\mathbf{L}_{ss}^0, \mathbf{M}_{sr}^0, \mathbf{I}_r, \mathbf{I}_s, \mathbf{U}_s$ and \mathbf{U}_r are matrices with the self and mutual inductance, stator and rotor currents and voltages values associated to inductance, current and voltage harmonics
- R_s and R_r the stator and rotor resistances

In the bellow equations, indexes of factors (inductances and currents) are strictly defined and correspond to the algebraic multiple of the angular velocity.

4.2 HBM: Dynamic Eccentricity Model (Machine with $p=2$)

$$\begin{aligned}
 & \left[\begin{array}{c} \vdots \\ (\Omega_0 + 4\Omega) \cdot E \\ (\Omega_0 + 3\Omega) \cdot E \\ (\Omega_0 + 2\Omega) \cdot E \\ (\Omega_0 + \Omega) \cdot E \\ \Omega_0 \cdot E \\ (\Omega_0 - \Omega) \cdot E \\ (\Omega_0 - 2\Omega) \cdot E \\ (\Omega_0 - 3\Omega) \cdot E \\ (\Omega_0 - 4\Omega) \cdot E \\ \vdots \end{array} \right] \cdot \text{diag} \left[\begin{array}{c} \vdots \\ j \\ \vdots \end{array} \right] \\
 & + \left[\begin{array}{c} \vdots \\ (\Omega_0 + 4\Omega) \cdot E \\ (\Omega_0 + 3\Omega) \cdot E \\ (\Omega_0 + 2\Omega) \cdot E \\ (\Omega_0 + \Omega) \cdot E \\ \Omega_0 \cdot E \\ (\Omega_0 - \Omega) \cdot E \\ (\Omega_0 - 2\Omega) \cdot E \\ (\Omega_0 - 3\Omega) \cdot E \\ (\Omega_0 - 4\Omega) \cdot E \\ \vdots \end{array} \right] \cdot \text{diag} \left[\begin{array}{c} \vdots \\ j \\ \vdots \end{array} \right] \\
 & \left[\begin{array}{cccccccc} \vdots & \vdots & \vdots & \vdots & \vdots & \vdots & \vdots & \vdots \\ \dots & L_{ss}^0 & 0 & 0 & 0 & L_{ss}^4 & 0 & 0 & 0 & 0 & \dots \\ \dots & 0 & L_{ss}^0 & 0 & 0 & 0 & L_{ss}^4 & 0 & 0 & 0 & \dots \\ \dots & 0 & 0 & L_{ss}^0 & 0 & 0 & 0 & L_{ss}^4 & 0 & 0 & \dots \\ \dots & 0 & 0 & 0 & L_{ss}^0 & 0 & 0 & 0 & L_{ss}^4 & 0 & \dots \\ \dots & L_{ss}^{-4} & 0 & 0 & 0 & L_{ss}^0 & 0 & 0 & 0 & L_{ss}^4 & \dots \\ \dots & 0 & L_{ss}^{-4} & 0 & 0 & 0 & L_{ss}^0 & 0 & 0 & 0 & \dots \\ \dots & 0 & 0 & L_{ss}^{-4} & 0 & 0 & 0 & L_{ss}^0 & 0 & 0 & \dots \\ \dots & 0 & 0 & 0 & L_{ss}^{-4} & 0 & 0 & 0 & L_{ss}^0 & 0 & \dots \\ \dots & 0 & 0 & 0 & 0 & L_{ss}^{-4} & 0 & 0 & 0 & L_{ss}^0 & \dots \\ \vdots & \vdots & \vdots & \vdots & \vdots & \vdots & \vdots & \vdots & \vdots & \vdots & \vdots \end{array} \right] \\
 & \left[\begin{array}{cccccccc} \vdots & \vdots & \vdots & \vdots & \vdots & \vdots & \vdots & \vdots \\ \dots & 0 & 0 & M_{sr}^2 & 0 & 0 & 0 & 0 & 0 & 0 & \dots \\ \dots & 0 & 0 & 0 & M_{sr}^2 & 0 & 0 & 0 & 0 & 0 & \dots \\ \dots & M_{sr}^{-2} & 0 & 0 & 0 & M_{sr}^2 & 0 & 0 & 0 & 0 & \dots \\ \dots & 0 & M_{sr}^{-2} & 0 & 0 & 0 & M_{sr}^2 & 0 & 0 & 0 & \dots \\ \dots & 0 & 0 & 0 & M_{sr}^{-2} & 0 & 0 & 0 & M_{sr}^2 & 0 & \dots \\ \dots & 0 & 0 & 0 & 0 & M_{sr}^{-2} & 0 & 0 & 0 & M_{sr}^2 & \dots \\ \dots & 0 & 0 & 0 & 0 & 0 & M_{sr}^{-2} & 0 & 0 & 0 & \dots \\ \dots & 0 & 0 & 0 & 0 & 0 & 0 & M_{sr}^{-2} & 0 & 0 & \dots \\ \vdots & \vdots & \vdots & \vdots & \vdots & \vdots & \vdots & \vdots & \vdots & \vdots & \vdots \end{array} \right] \\
 & \left[\begin{array}{cccccccc} \vdots & \vdots & \vdots & \vdots & \vdots & \vdots & \vdots & \vdots \\ \dots & L_{rr}^0 & 0 & 0 & 0 & 0 & 0 & 0 & 0 & 0 & \dots \\ \dots & 0 & L_{rr}^0 & 0 & 0 & 0 & 0 & 0 & 0 & 0 & \dots \\ \dots & 0 & 0 & L_{rr}^0 & 0 & 0 & 0 & 0 & 0 & 0 & \dots \\ \dots & 0 & 0 & 0 & L_{rr}^0 & 0 & 0 & 0 & 0 & 0 & \dots \\ \dots & 0 & 0 & 0 & 0 & L_{rr}^0 & 0 & 0 & 0 & 0 & \dots \\ \dots & 0 & 0 & 0 & 0 & 0 & L_{rr}^0 & 0 & 0 & 0 & \dots \\ \dots & 0 & 0 & 0 & 0 & 0 & 0 & L_{rr}^0 & 0 & 0 & \dots \\ \dots & 0 & 0 & 0 & 0 & 0 & 0 & 0 & L_{rr}^0 & 0 & \dots \\ \vdots & \vdots & \vdots & \vdots & \vdots & \vdots & \vdots & \vdots & \vdots & \vdots & \vdots \end{array} \right] \\
 & + \left[\begin{array}{c} \vdots \\ R_s \\ R_s \\ R_s \\ R_s \\ R_s \\ R_s \\ R_s \\ R_s \\ R_s \\ R_s \\ \vdots \end{array} \right] \cdot \text{diag} \left[\begin{array}{c} \vdots \\ \vdots \\ \vdots \\ \vdots \\ \vdots \\ \vdots \\ \vdots \\ \vdots \\ \vdots \\ \vdots \\ \vdots \\ \vdots \end{array} \right] \\
 & \left[\begin{array}{c} \vdots \\ R_r \\ R_r \\ R_r \\ R_r \\ R_r \\ R_r \\ R_r \\ R_r \\ R_r \\ R_r \\ \vdots \end{array} \right] \cdot \text{diag} \left[\begin{array}{c} \vdots \\ \vdots \\ \vdots \\ \vdots \\ \vdots \\ \vdots \\ \vdots \\ \vdots \\ \vdots \\ \vdots \\ \vdots \\ \vdots \end{array} \right] \\
 & \left[\begin{array}{c} \vdots \\ I_{s,4} \\ I_{s,3} \\ I_{s,2} \\ I_{s,1} \\ I_{s,0} \\ I_{s,-1} \\ I_{s,-2} \\ I_{s,-3} \\ I_{s,-4} \\ \vdots \end{array} \right] = \left[\begin{array}{c} \vdots \\ U \\ \vdots \end{array} \right]
 \end{aligned}$$

(4.3)

As it happens with the SE model, DE can also be reduced as only a few element are coupled by the voltage harmonics "U". However, the harmonic of the stator and rotor currents are different (linked to different omega pulsations). The resultant model corresponds to the electrical equations of the DE model presented in chapter 3.

L_{ss} , M_{sr} and I_s , I_r are the specific inductance and current values couple by the voltage harmonic.

$$\left[\begin{array}{c} \text{diag} \left(\begin{array}{c} j \cdot \Omega_0 \\ j \cdot (\Omega_0 - 2p\Omega) \end{array} \right) \\ \text{diag} \left(\begin{array}{c} j \cdot (\Omega_0 - 2\Omega) \\ j \cdot (\Omega_0 - 2\Omega) \end{array} \right) \end{array} \right] \cdot \left[\begin{array}{cccc} L_{ss1} & L_{ss2} & M_{sr1} & M_{sr2} \\ L_{ss2} & L_{ss1} & M_{sr2} & M_{sr1} \\ M_{sr1} & M_{sr2} & L_{rr1} & L_{rr2} \\ M_{sr2} & M_{sr1} & L_{rr2} & L_{rr1} \end{array} \right] + \left[\begin{array}{c} \text{diag} \left[\begin{array}{c} R_s \\ R_s \end{array} \right] \\ \text{diag} \left[\begin{array}{c} R_r \\ R_r \end{array} \right] \end{array} \right] \cdot \left[\begin{array}{c} I_{s,0} \\ I_{s,-4} \\ I_{r,-2} \\ I_{r,-2} \end{array} \right] = \left[\begin{array}{c} U_1 \\ 0 \\ 0 \\ 0 \end{array} \right] \quad (4.4)$$

4.3 HBM: Mixed Eccentricity Model

$$\begin{aligned}
 & \left[\begin{array}{c} \vdots \\ \Omega_0 + 4\Omega \\ \Omega_0 + 3\Omega \\ \Omega_0 + 2\Omega \\ \Omega_0 + \Omega \\ \Omega_0 \\ \Omega_0 - \Omega \\ \Omega_0 - 2\Omega \\ \Omega_0 - 3\Omega \\ \Omega_0 - 4\Omega \\ \vdots \end{array} \right] \cdot \text{diag } j \cdot \left[\begin{array}{c} \vdots \\ \vdots \\ \vdots \\ \vdots \\ \vdots \\ \vdots \\ \vdots \\ \vdots \\ \vdots \\ \vdots \\ \vdots \end{array} \right] + \left[\begin{array}{cccccccc} \vdots & \vdots & \vdots & \vdots & \vdots & \vdots & \vdots & \vdots \\ \dots & L_{ss}^0 & L_{ss}^1 & L_{ss}^2 & 0 & 0 & 0 & 0 \\ \dots & L_{ss}^{-1} & L_{ss}^0 & L_{ss}^1 & L_{ss}^2 & 0 & 0 & 0 \\ \dots & L_{ss}^{-2} & L_{ss}^{-1} & L_{ss}^0 & L_{ss}^1 & L_{ss}^2 & 0 & 0 \\ \dots & 0 & L_{ss}^{-2} & L_{ss}^{-1} & L_{ss}^0 & L_{ss}^1 & L_{ss}^2 & 0 \\ \dots & 0 & 0 & L_{ss}^{-2} & L_{ss}^{-1} & L_{ss}^0 & L_{ss}^1 & L_{ss}^2 \\ \dots & 0 & 0 & 0 & L_{ss}^{-2} & L_{ss}^{-1} & L_{ss}^0 & L_{ss}^1 \\ \dots & 0 & 0 & 0 & 0 & L_{ss}^{-2} & L_{ss}^{-1} & L_{ss}^0 \\ \dots & 0 & 0 & 0 & 0 & 0 & L_{ss}^{-2} & L_{ss}^{-1} \\ \vdots & \vdots & \vdots & \vdots & \vdots & \vdots & \vdots & \vdots \end{array} \right] + \left[\begin{array}{cccccccc} \vdots & \vdots & \vdots & \vdots & \vdots & \vdots & \vdots & \vdots \\ \dots & M_{sr}^0 & M_{sr}^1 & M_{sr}^2 & M_{sr}^3 & M_{sr}^4 & 0 & 0 \\ \dots & M_{sr}^{-1} & M_{sr}^0 & M_{sr}^1 & M_{sr}^2 & M_{sr}^3 & M_{sr}^4 & 0 \\ \dots & M_{sr}^{-2} & M_{sr}^{-1} & M_{sr}^0 & M_{sr}^1 & M_{sr}^2 & M_{sr}^3 & M_{sr}^4 \\ \dots & M_{sr}^{-3} & M_{sr}^{-2} & M_{sr}^{-1} & M_{sr}^0 & M_{sr}^1 & M_{sr}^2 & M_{sr}^3 \\ \dots & M_{sr}^{-4} & M_{sr}^{-3} & M_{sr}^{-2} & M_{sr}^{-1} & M_{sr}^0 & M_{sr}^1 & M_{sr}^2 \\ \dots & 0 & M_{sr}^{-4} & M_{sr}^{-3} & M_{sr}^{-2} & M_{sr}^{-1} & M_{sr}^0 & M_{sr}^1 \\ \dots & 0 & 0 & M_{sr}^{-4} & M_{sr}^{-3} & M_{sr}^{-2} & M_{sr}^{-1} & M_{sr}^0 \\ \dots & 0 & 0 & 0 & M_{sr}^{-4} & M_{sr}^{-3} & M_{sr}^{-2} & M_{sr}^{-1} \\ \vdots & \vdots & \vdots & \vdots & \vdots & \vdots & \vdots & \vdots \end{array} \right] + \left[\begin{array}{cccccccc} \vdots & \vdots & \vdots & \vdots & \vdots & \vdots & \vdots & \vdots \\ \dots & L_{rr}^0 & L_{rr}^1 & L_{rr}^2 & L_{rr}^3 & L_{rr}^4 & L_{rr}^5 & L_{rr}^6 \\ \dots & L_{rr}^{-1} & L_{rr}^0 & L_{rr}^1 & L_{rr}^2 & L_{rr}^3 & L_{rr}^4 & L_{rr}^5 \\ \dots & L_{rr}^{-2} & L_{rr}^{-1} & L_{rr}^0 & L_{rr}^1 & L_{rr}^2 & L_{rr}^3 & L_{rr}^4 \\ \dots & L_{rr}^{-3} & L_{rr}^{-2} & L_{rr}^{-1} & L_{rr}^0 & L_{rr}^1 & L_{rr}^2 & L_{rr}^3 \\ \dots & L_{rr}^{-4} & L_{rr}^{-3} & L_{rr}^{-2} & L_{rr}^{-1} & L_{rr}^0 & L_{rr}^1 & L_{rr}^2 \\ \dots & L_{rr}^{-5} & L_{rr}^{-4} & L_{rr}^{-3} & L_{rr}^{-2} & L_{rr}^{-1} & L_{rr}^0 & L_{rr}^1 \\ \dots & L_{rr}^{-6} & L_{rr}^{-5} & L_{rr}^{-4} & L_{rr}^{-3} & L_{rr}^{-2} & L_{rr}^{-1} & L_{rr}^0 \\ \dots & 0 & L_{rr}^{-6} & L_{rr}^{-5} & L_{rr}^{-4} & L_{rr}^{-3} & L_{rr}^{-2} & L_{rr}^{-1} \\ \dots & 0 & 0 & L_{rr}^{-6} & L_{rr}^{-5} & L_{rr}^{-4} & L_{rr}^{-3} & L_{rr}^{-2} \\ \vdots & \vdots & \vdots & \vdots & \vdots & \vdots & \vdots & \vdots \end{array} \right] + \text{diag } R_s \cdot \left[\begin{array}{c} \vdots \\ R_s \\ R_s \\ R_s \\ R_s \\ R_s \\ R_s \\ R_s \\ R_s \\ R_s \\ \vdots \end{array} \right] + \left[\begin{array}{c} \vdots \\ I_{s,4} \\ I_{s,3} \\ I_{s,2} \\ I_{s,1} \\ I_{s,0} \\ I_{s,-1} \\ I_{s,-2} \\ I_{s,-3} \\ I_{s,-4} \\ \vdots \end{array} \right] = \left[\begin{array}{c} \vdots \\ R_r \\ R_r \\ R_r \\ R_r \\ R_r \\ R_r \\ R_r \\ R_r \\ R_r \\ \vdots \end{array} \right] \cdot \text{diag } j \cdot \left[\begin{array}{c} \vdots \\ \vdots \\ \vdots \\ \vdots \\ \vdots \\ \vdots \\ \vdots \\ \vdots \\ \vdots \\ \vdots \\ \vdots \end{array} \right] + \left[\begin{array}{c} \vdots \\ I_{r,4} \\ I_{r,3} \\ I_{r,2} \\ I_{r,1} \\ I_{r,0} \\ I_{r,-1} \\ I_{r,-2} \\ I_{r,-3} \\ I_{r,-4} \\ \vdots \end{array} \right] = \left[\begin{array}{c} \vdots \\ 0 \\ 0 \\ 0 \\ 0 \\ 0 \\ 0 \\ 0 \\ 0 \\ 0 \\ \vdots \end{array} \right] + U \cdot \left[\begin{array}{c} \vdots \\ 0 \\ 0 \\ 0 \\ 0 \\ 0 \\ 0 \\ 0 \\ 0 \\ 0 \\ \vdots \end{array} \right]
 \end{aligned}$$

(4.5)

Nevertheless, from the model in natural components of ME, it is easy to obtain the SE and DE models understanding the physical phenomena. For SE the position of the minimal air-gap does not depend on “ φ ”, but only on “ x ”. By only considering the main Fourier coefficients, Λ_0 , Λ_{2p} and Λ_p , and the harmonic “ $m=0$ ” in equations 3.120, 3.121 and 3.122, the model of SE can be found. For DE, apart from the considerations taken for the SE model the angle “ γ ” has to be substituted for “ $\delta+\varphi$ ” where δ is the initial position of the minimal air-gap. For DE, the position of the minimal air-gap depends on the rotational angle “ φ ”.

Chapter 5 Matlab/Simulink Implementation of Dynamic Induction Motor Models

The aim of the thesis is developing dynamic models of IM for drives applications which accounts the effects of main MMFs. They will be used to study the interactions of drive polities running fault machines in order to develop new control laws. In this chapter dynamic models of induction motor for drives applications are presented including some of the model’s results.

Drives application are usually employed for signal processing of measurements or control applications. The implementation of the algorithms and dynamic systems involved are naturally discrete-time as the computer execute and collect data in discrete points of the time, for instance, observers, state estimator as KF or filters. Due to the fact that models develop in the thesis are non-linear (the state space variables depends on the speed rotor or stator speed) the Euler’s forward method has been selected. Additionally this method allows to find an explicit formula of output (e.g., stator and rotor currents or fluxes).

Some of the Simulink model are discussed below:

5.1 Healthy Induction Motor Model

The healthy induction motor model has been used as a reference to analyze the differences between the electrical machine signatures from each model. Fault models have been developed based on the classical mathematical model of IM, which means, they are constituted by four electrical equations and two mechanical equations (with the exception of the steady state model of ME).

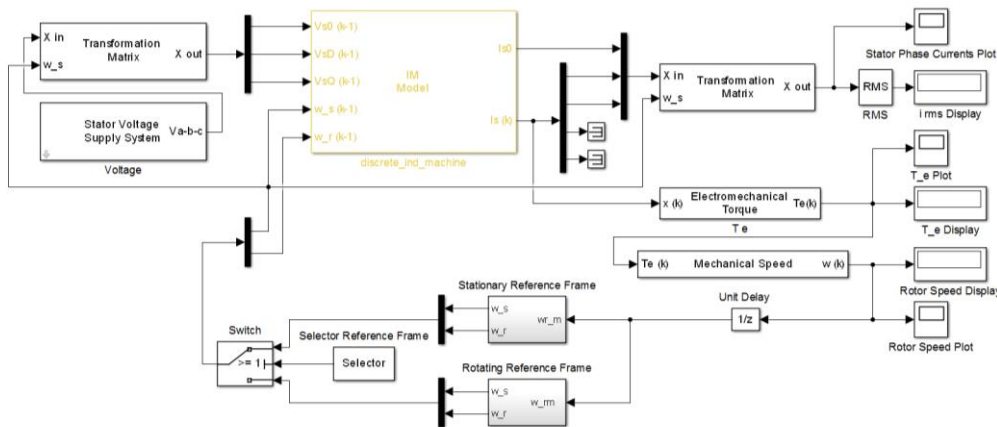


Fig. 5.1 Simulink model of healthy induction motor

Fig. 5.1 shows the Simulink model of healthy IM. The Structure of the model is as follows:

- Stator Voltage Supply System Block: definition of the supply voltages
- Transformation Matrix Block: the transformation matrices used to simplify the electrical equations (and the inverse matrix).
- IM Model Block: definition of the electrical motor equations based on models from Chapter 3.
- Electromechanical Torque Block: calculation of the electromechanical torque
- Mechanical Speed Block: solving the mechanical equation.

Summary “Simulink models of faulty induction machines for drives applications”

- Selector Reference Frame Switch: stationary or rotating reference frame selector.

The healthy model has been tested for the motor T-DF112M-4 with sampling time “ $T_s = 1e^{-5}$ ”, 120% of the load torque (12.4 Nm). The results are shown below:

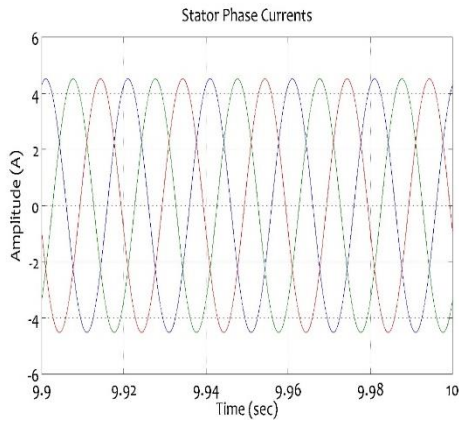


Fig. 5.2 HM stator phase currents

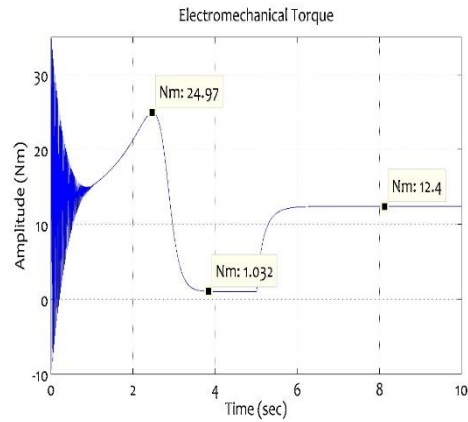


Fig. 5.3 HM electromagnetic torque

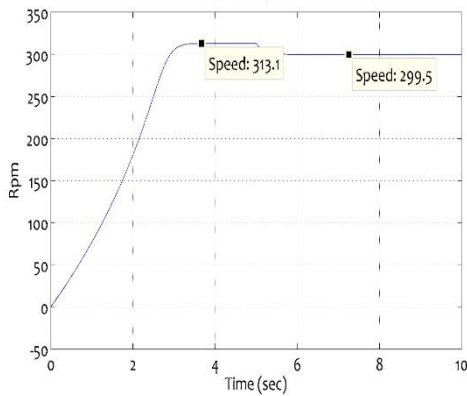


Fig. 5.4 HM rotor speed

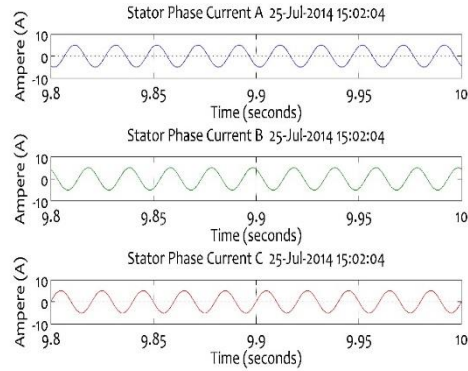


Fig. 5.5 Stator Phase Currents

The above results agree with the real values of the motor.

5.2 Dynamic Eccentricity Induction Motor Model

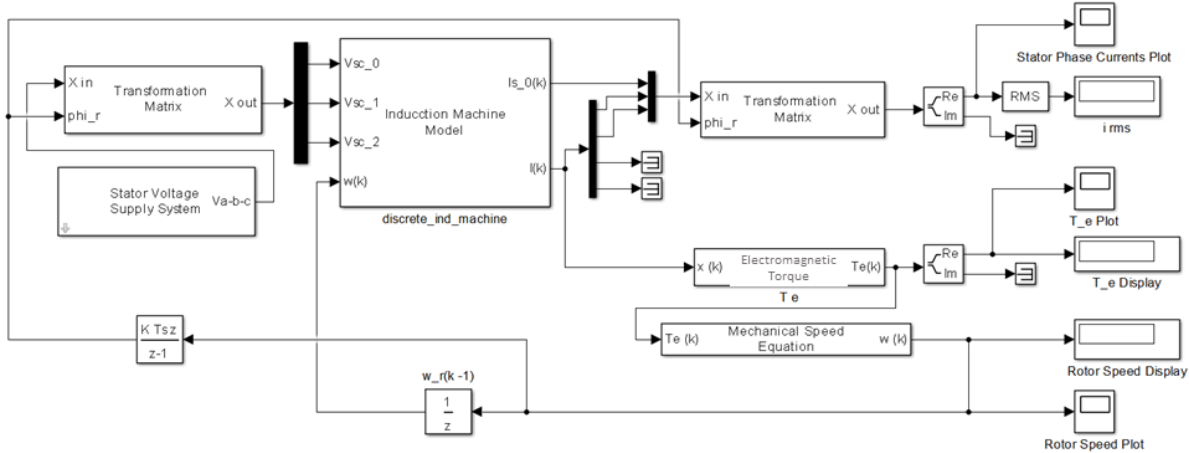


Fig. 5.6 Simulink model of DE induction motor

Fig. 5.6 shows the model of Dynamic Eccentricity (DE) Induction Motor. It contains the same blocks and the

Summary “Simulink models of faulty induction machines for drives applications”

results shown below have been tested in the same conditions as the Healthy Machine, however, this model does not have the possibility of changing the reference frame because the transformation applied to simplify the model requires a specific angle and the IM Model block contains the equations for DE. Moreover, the positive and negative sequence of the currents and voltages can be obtained from the model. A 40% of DE has been tested:

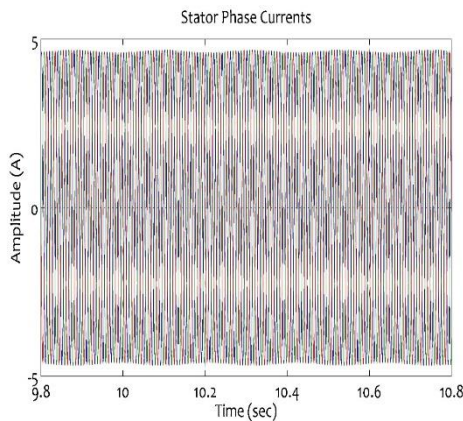


Fig. 5.7 DE stator phase currents

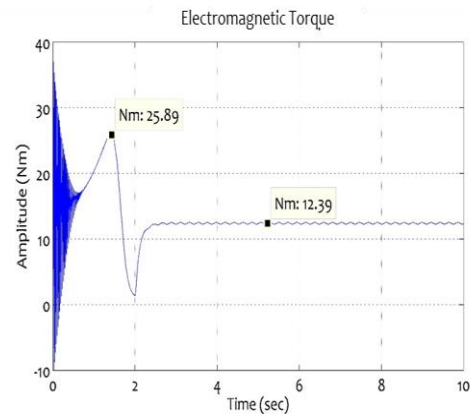


Fig. 5.8 DE electromagnetic torque

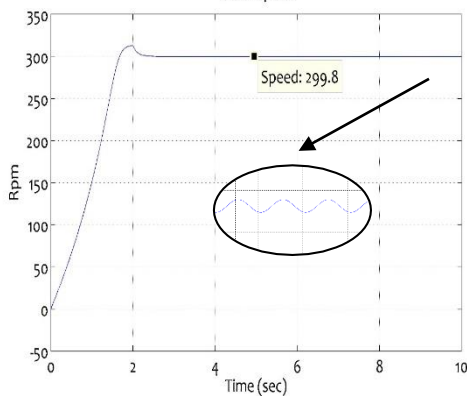


Fig. 5.9 DE rotor speed

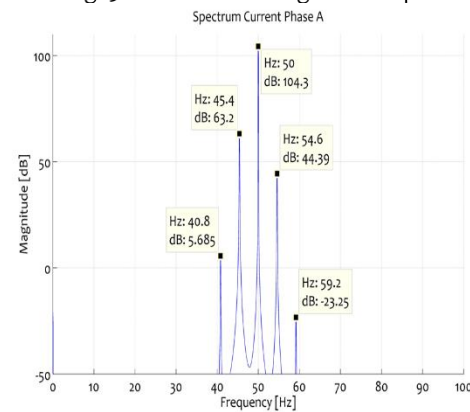


Fig. 5.10 Current spectra DE induction motor

In Fig. 5.7 it can be distinguished the characteristic ripple associated to the fault. DE produces similar effects as BB fault. Sidebands $(1 - 2s)f_0$ also arise in the frequency spectra because the model includes the mechanical equation. In case of DE, according the performance of the motor, the amplitude of the sidebands varies. Chapter 7 compares the dynamic model and the static model results with the measurement and analyses the behavior of the sidebands.

Chapter 6 Matlab Implementation of Steady State Induction Motor Models

The simplification of the mathematical equations cannot be always accomplished due to the nature of the fault. This is the case of ME which self-inductance and mutual inductance matrices depend on the angular position of the rotor. As those inductance are not constant matrices, the model of IM for ME cannot be found as it happens for SE, DE or BB faults (Discussed on the Chapter 3 of the thesis). However, the spectra of the stator phase currents can be obtained for the steady state operation points applying the HBM (Chapter 4).

In the present chapter the stator current spectra for SE, DE and ME models in frequency domain will be discussed by means of the FFT. Additionally, it will be explained how the stator currents in time domain are calculated for each eccentricity fault as a function of the current and speed harmonics. The squirrel cage motor has been

Summary “Simulink models of faulty induction machines for drives applications”

models as a rotor winding induction motor applying the assumption of stator and rotor windings are equal.

For instance, the stator currents in time domain of the DE model are calculated as follows:

The HBM is solved considering only the voltage harmonic with pulsation Ω_0 ,

$$U_\eta = \frac{U_n}{2} \cdot e^{j \cdot (\Omega_0) \cdot t} + \frac{U_n}{2} \cdot e^{j \cdot (-\Omega_0) \cdot t} \quad (6.1)$$

Only two current harmonics are different than zero:

$$\begin{bmatrix} I_{sc0}^{DE}(t) \\ I_{sc1}^{DE}(t) \\ I_{sc2}^{DE}(t) \end{bmatrix} = \begin{bmatrix} 0 \\ I_1^{DE} \\ 0 \end{bmatrix} \cdot e^{j \cdot (\Omega_0) \cdot t} + \begin{bmatrix} 0 \\ 0 \\ I_2^{DE} \end{bmatrix} \cdot e^{j \cdot (\Omega_0 - 2p\Omega_m) \cdot t}; \left(\text{for } \frac{U_n}{2} \cdot e^{j \cdot (\Omega_0) \cdot t} \right); \quad (6.2)$$

Applying the principle of superposition, the current harmonics for the voltage harmonic with pulsation $-\Omega_0$ are,

$$\begin{bmatrix} I_{sc0}^{DE}(t) \\ I_{sc1}^{DE}(t) \\ I_{sc2}^{DE}(t) \end{bmatrix} = \begin{bmatrix} 0 \\ 0 \\ I_1^{DE} \end{bmatrix} \cdot e^{j \cdot (-\Omega_0) \cdot t} + \begin{bmatrix} 0 \\ I_2^{DE} \\ 0 \end{bmatrix} \cdot e^{-j \cdot (\Omega_0 - 2p\Omega_m) \cdot t}; \left(\text{for } \frac{U_n}{2} \cdot e^{j \cdot (-\Omega_0) \cdot t} \right); \quad (6.3)$$

The backward and forward symmetrical component can be found as:

$$\begin{bmatrix} I_{sc0}^{DE}(t) \\ I_{sc1}^{DE}(t) \\ I_{sc2}^{DE}(t) \end{bmatrix} = \begin{bmatrix} 0 \\ I_1^{DE} \cdot e^{j \cdot (\Omega_0) \cdot t} \\ I_1^{DE} \cdot e^{j \cdot (-\Omega_0) \cdot t} \end{bmatrix} + \begin{bmatrix} 0 \\ I_2^{DE} \cdot e^{-j \cdot (\Omega_0 - 2p\Omega_m) \cdot t} \\ I_2^{DE} \cdot e^{j \cdot (\Omega_0 - 2p\Omega_m) \cdot t} \end{bmatrix}; \text{for } (U_\eta, \eta = \pm 1); \quad (6.4)$$

From equation 6.4 it can be proved that backward symmetrical component is equal to the conjugate forward symmetrical component:

$$I_{sc2}^{DE} = \overline{I_{sc1}^{DE}} \quad (6.5)$$

Finally, the time domain stator currents are obtained applying the inverse SC transformation matrix:

$$\begin{bmatrix} I_a^{DE}(t) \\ I_b^{DE}(t) \\ I_c^{DE}(t) \end{bmatrix} = \frac{1}{\sqrt{3}} \cdot \begin{bmatrix} 1 & 1 & 1 \\ 1 & a^2 & a \\ 1 & a & a^2 \end{bmatrix} \cdot \begin{bmatrix} I_{sc0}^{DE}(t) \\ I_{sc1}^{DE}(t) \\ I_{sc2}^{DE}(t) \end{bmatrix} \quad (6.6)$$

This chapter includes simulations of the motor model “T-DF112M-4” with different levels of eccentricity for all eccentricity types. In order to present the content, this summary shows only one of the models discussed:

1. DE static model tested with 40% of eccentricity

6.1 Simulation of 40% DE static model

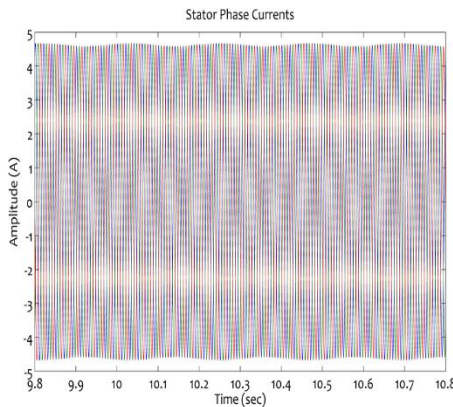


Fig. 6.1 Stator phase current waveform DE

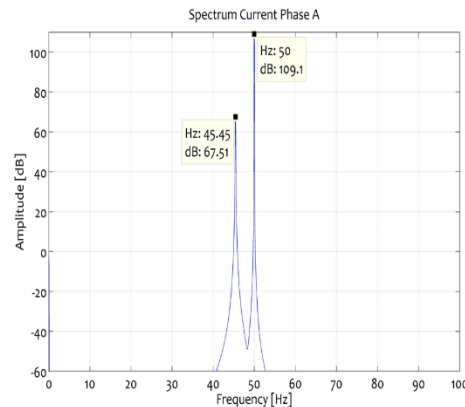


Fig. 6.2 Frequency spectra of stator phase currents DE

The above figures show the frequency spectra and the waveform of the stator phase currents obtained from the model. The current frequency spectra shows the characteristic left sideband associated to the electrical equation of the converter. In chapter 5 it can be appreciated how the right band appears due to solving the

Summary “Simulink models of faulty induction machines for drives applications”

mechanical equation. Furthermore, it can also be seen the ripple on the stator phase currents characteristic of this type of faults. As it was mentioned, the simulation results are discussed based on the measurement results on chapter 7.

Chapter 7 Validation of Model Results by Experimental Test

In the previous chapter, the dynamic and static models for DE were presented and the simulation results were showed. The simulation results agree with the expected values of the real machine when it is affected by those faults, for instance, the additional frequencies on the stator phase currents. However, the final validation is done by studying the evolution of the sidebands when the motor is working under different conditions.

7.1 Dynamic Eccentricity (DE): Measurement Results

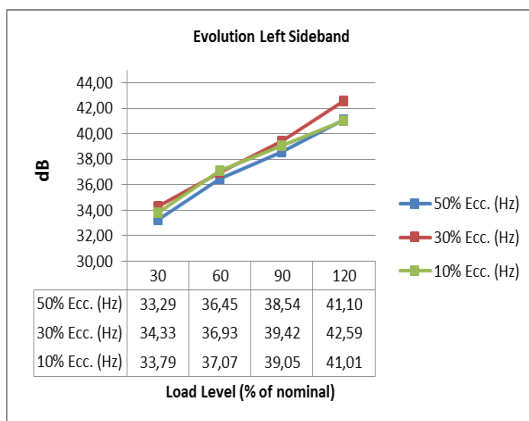


Fig. 7.1 DE Evolution Left Sideband – Experiments

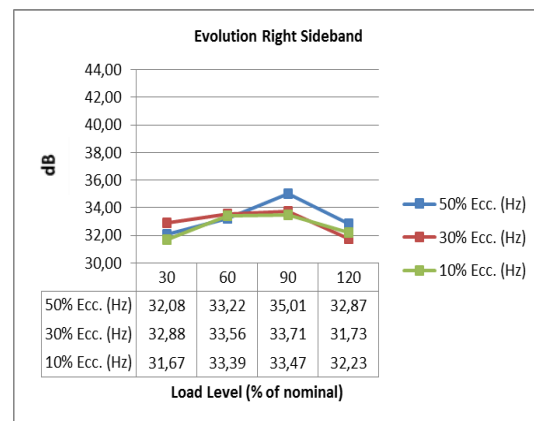


Fig. 7.2 DE Evolution Right Sideband – Experiments

According to the experimental data, the amplitude of both sidebands for each level of load does not depend on the level of eccentricity, however, it can be observed how the left sideband amplitude increases and the right sideband amplitude decreases with the load. Those values agree with the expected evolution of DE.

7.2 Dynamic Eccentricity (DE) Dynamic Model: Simulation Results

The simulation results show the evolution of the sidebands amplitude for different levels of eccentricity:

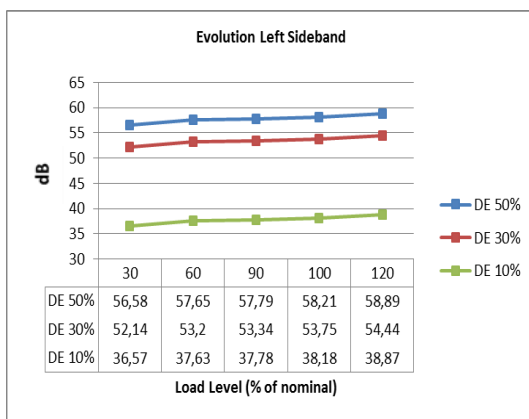


Fig. 7.3 DE Evolution Left Sideband – Simulation Dynamic Model

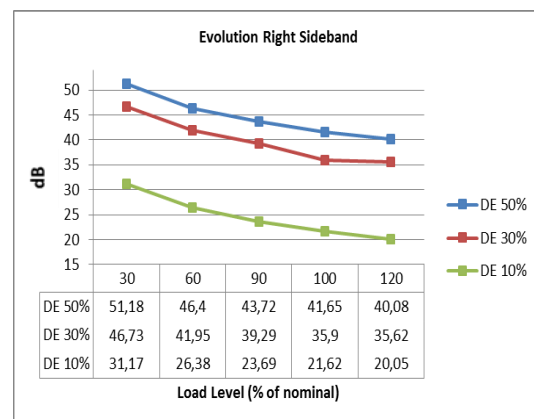


Fig. 7.4 DE Evolution Right Sideband – Simulation Dynamic Model

Summary “Simulink models of faulty induction machines for drives applications”

The simulation results show a similar evolution of the sidebands amplitude, however the differences in magnitudes are higher because the estimation of the machine inductance is not accurate enough.

7.1 Dynamic Eccentricity (DE) Static Model: Simulation Results

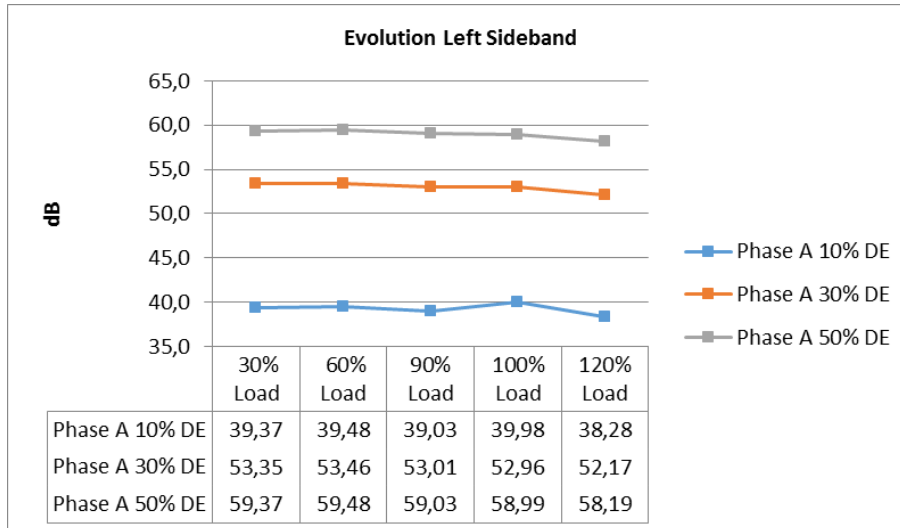


Fig. 7.5 Evolution Left Sideband HBM DE

Comparing the simulation results of DE between dynamic models and steady state models slight variations of the harmonics as well as in the trends can be observed. The solution of the mechanical and electrical equations implies that the left sideband increases with the load but magnitudes remains lower than steady state results. Regardless of those differences, both models fulfil all the requirements according to the assumptions taken and agree with the measurement results.

7.2 Conclusions on the Model's Performance

It is worth to mention the conclusions reached by the analysis done in the thesis regarding the performance of all models (dynamic and static).

The results have shown a correct performance of the models. The frequency analysis of the stator phase currents in all models present the characteristic additional frequencies. For steady state simulations, the frequencies associated with the mechanical side of the system do not appear. The evolution of the sidebands around the main harmonic (50 Hz) agrees with experimental data for different load conditions and fault severities. On the other hand, if the user seeks a quantitative analysis of faults, some of the following action may be considered in order to obtain a better estimation of the machine parameters for each operation point:

- Saturation coefficients calculated by FEM model for each level of load
- Design of EKF which estimates the healthy machine parameters for different load conditions
- Consider saturation and slot effects in the calculation of the permeance function
- Estimation of saturation coefficients as function of the main inductance calculated by formulas and the estimated by experiments for each level of load
- Estimation of rotor cage resistance variation due to eddy currents

Summary “Simulink models of faulty induction machines for drives applications”

In conclusion, the dynamic and steady models presented in the thesis demonstrate that a qualitative analysis of faults can be carried out by only considering MMFs effects fulfilling all requirements needed for drives applications as the tendencies shown in simulations match the experimental data.

Chapter 8 Drives Applications with Faulty Induction Motor models: Hardware in the Loop Simulations HIL

In the past the construction of prototypes was a common practice during the test phase of new ideas/concepts and products. This testing stage required long periods of time and the investment of many resources. Another important factor was the safety during the tests as the operators could suffer accidents. In the past few decades, the evolution of the computers and the development of new platforms for modelling implementation have helped to reduce the time invested to transform an idea into a product, the total cost of the whole process and have improved the work conditions decreasing the risk of prospective accidents.

Hardware in the loop simulation (HIL) techniques have been developed to speed up the test and development process of embedded systems. Those techniques provide a platform to study the interaction between real-times embedded systems, such as power electronic control systems, with a “plant” (electrical motors), represented by complex mathematical models.

Power electronic control simulations require high-speed digital processors which reproduce the fast dynamic responses due to the high frequency switching actions of the power electronic switches. Real-time simulations can be satisfied thanks to the FPGA/CPU platforms used for HIL.

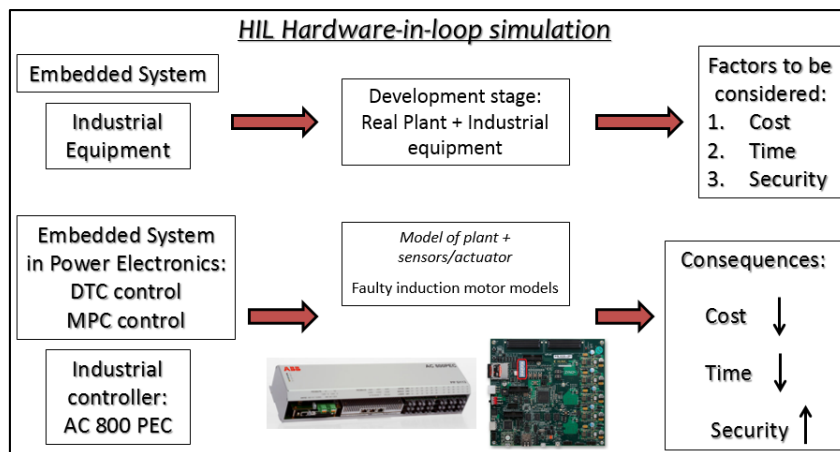


Fig. 8.1 HIL vs old approach

Model develop in the thesis were implement in real drives applications at ABB Research Cooperative Center – Poland within the Energy Smartops activities program with positive results.

8.1 Implementation of Healthy Induction Motor model into Zynq-7000 All Programmable SoC - Discussion of Results

Following figures show supply voltages, electromagnetic torque and rotor speed signals calculated by ZYNQ during the execution of the Healthy machine model (Fig. 8.4 / Fig. 8.5) and BB model (Fig. 8.6 / Fig. 8.7) running at the same operation point, using the stationary reference frame and expressed in d-q components. The magnitude and behaviour of the machine signatures were equal to the simulation results obtained in Simulink after applying the proper scale factors.



Fig. 8.4 Supply voltages in D-Q components for both Models

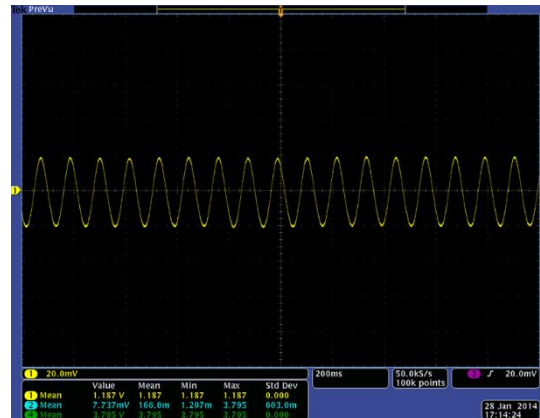


Fig. 8.5 Electromagnetic torque ripple cage asymmetry



Fig. 8.6 Electro-mechanical torque (Yellow) and electrical rotor speed (Blue) healthy machine

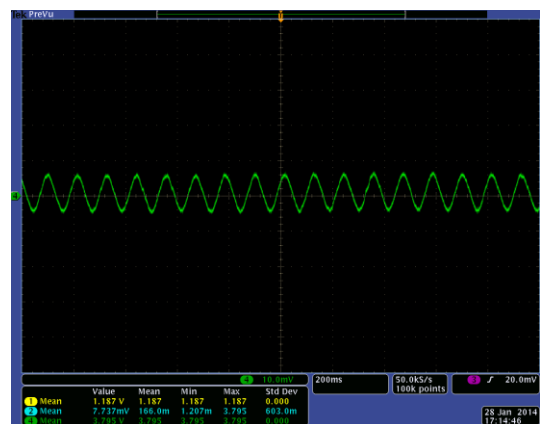


Fig. 8.7 Electrical rotor speed ripple cage asymmetry

Chapter 9 Analysis and Diagnosis of Electrical and Mechanical Faults in Induction Motors

The content of this chapter summarizes some of the work carried out in the field of fault diagnosis of IMs through simulation and experimental data.

9.1 *Evaluation of the Asymmetry Factor for BB Simulations Changes of simulation:* symmetry and asymmetry coefficient are used to model BB faults. Some of the assumptions taken in modelling are review as well as the evolution of their values for different faults.

Summary “Simulink models of faulty induction machines for drives applications”

9.2 *Diagnosis of Static Eccentricity vs Unbalance Supply Voltages*: difficulties in diagnosis of both faults are pointed out. Furthermore, a method to find differences is suggested.

9.3 *Modelling DE and Cage asymmetry*: the possibilities offer by combining BB and DE models for fault diagnosis purposes are investigated supported by experimental data.

9.4 *Comparison of Mechanical and Broken Bar Faults by means of Positive and Negative Frequency Spectrum of the Stator Phase Current in IM*: an alternative algorithm of Fourier transform has been applied in order to find differences between faults in the frequency spectra of the stator currents.

- *Interactions between Electrical and mechanical faults by means of MCSA*: study based on the evolution of the $(1 - 2s)f_0$ sidebands when an induction motor with BB is also affected by a mechanical fault with similar frequency range.

For example:

9.3 Modelling DE and Cage asymmetry

DE and BB faults are difficult to distinguish due to the fact that same sidebands around the main harmonic appear. In both cases the evolution of the sideband’s magnitudes is similar, for instance, regarding changes in the load. With the aim to bringing light to this challenge, mathematical models based on main MMFs may be used to study new algorithm of fault diagnosis. Three models have been tested: Model of BB, model of DE and a third one that combines the faults. The results obtained from all models in comparison with the experimental data reveals similar trends proving the suitability of the model for diagnosis purposes.

- Experimental Results

Once again, test performed in motor model T-DF112M-4 have shown differences in magnitude of the sidebands. Recalling chapter 8, the left sideband magnitude increases and the sideband magnitude decreases with the load for one BB and DE. Magnitude of sidebands for BB were higher than DE.

Experimental result when both fault occurs simultaneously shown the same trends with higher magnitudes than separated faults:

Table II Sideband magnitudes for DE + one BB / Experimental results

Dyn. Ecc. + one B.B. $(1-2s)f$	30% Load	60% Load	90% Load	120% Load
50	64.39	68.37	70.87	72.18
30	62.41	66.95	70.18	72.64
10	59.40	65.61	68.08	70.66
Dyn. Ecc. + one B.B. $(1+2s)f$	30% Load	60% Load	90% Load	120% Load
50	48.82	46.82	44.63	37.41
30	49.17	48.60	45.39	40.80
10	47.61	47.03	46.75	42.84

Summary “Simulink models of faulty induction machines for drives applications”

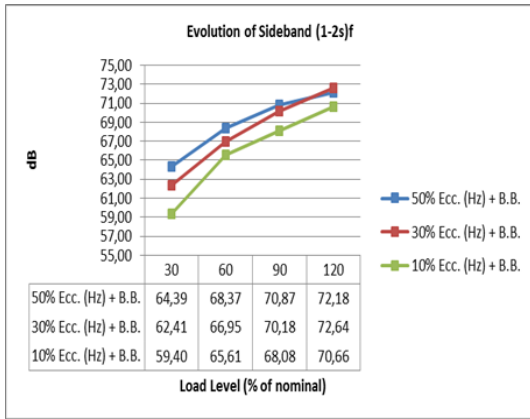


Fig. 9.1 Left sideband magnitude: DE + one BB / Experimental results

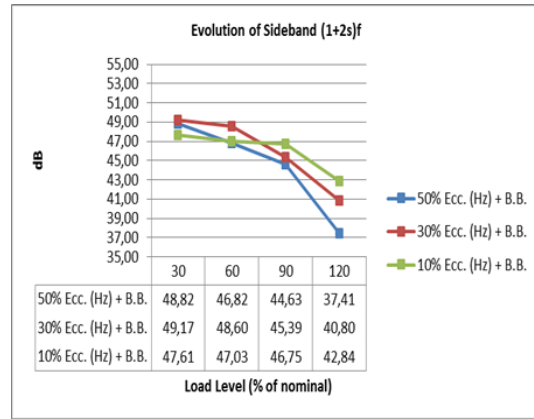


Fig. 9.2 Right sideband magnitude: DE + one BB / Experimental results

Regarding simulation results, it can be proven the same trends in the sidebands as well as the magnitudes values. Sorting from highest to lowest: DE + one BB / one BB / DE.

Table III Sideband magnitudes for DE + one BB / Simulation results

Dyn. Ecc. + one B.B. - (1-2s)f	30% Load	60% Load	90% Load	100% Load	120% Load
50	58.96	64.37	65.67	67.86	68.55
45	56.91	63.38	64.96	67.28	68.1
40	55.01	62.58	64.35	66.67	67.68
Dyn. Ecc. + one B.B. - (1+2s)f	30% Load	60% Load	90% Load	100% Load	120% Load
50	53.17	52.61	51.08	50.78	47.96
45	51.11	51.63	50.37	50.2	47.44
40	49.2	50.83	49.77	49.69	48.34

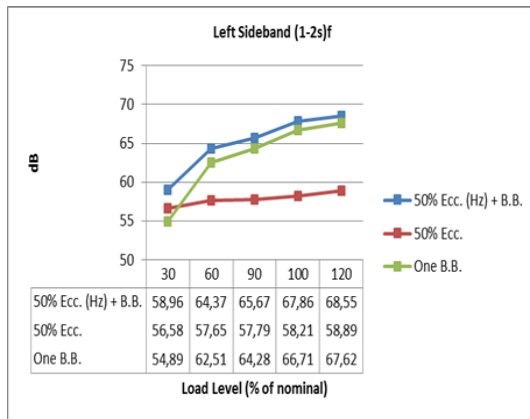


Fig. 9.3 Left sideband magnitude evolution for DE + one BB / Simulation results

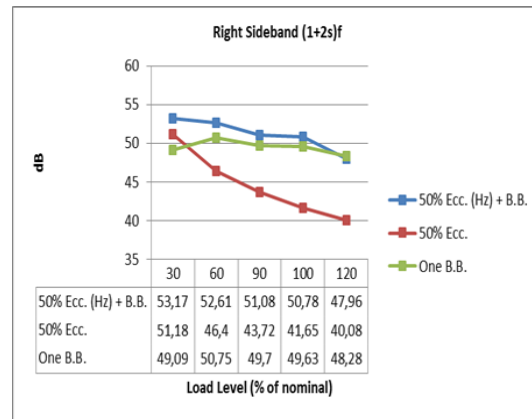


Fig. 9.4 Right sideband magnitude evolution for DE + one BB / Simulation results

It is true that differences between DE + one BB and BB fault are not big enough as it was shown in experimental results, but it is also true that parameters for estimation of BB may be not fully correct. In the light of results presented, it can be concluded that mono harmonic models accounting simultaneously BB and DE faults may be use for diagnosis purposes.

Chapter 10 Conclusions

The main contribution of the thesis has been the development of a library in Simulink of dynamic induction motor models under electrical and mechanical faults for drives applications. These model have been based on the

Summary “Simulink models of faulty induction machines for drives applications”

winding function approach for mathematical modelling of IMs accounting only effects of the main MMFs. Furthermore, steady state models accounting eccentricities faults have been created in Matlab following the HBM. The main advantage of the methodology presented is that it allows developing models of different types of electrical machines or considering effects of multi-harmonics. In addition, effects of saturation or slotting can be taken into account by adding additional terms to the permeance function. The research seeks a qualitative analysis of the electrical and mechanical faults by means of MCSA applied to the stator phase currents.

Simulation results shown in the thesis have mainly been focused in the analysis of the frequency spectra of the stator phase currents with the objective of studying the evolution of the characteristic frequencies for each type of fault. Performance of the models has been supported by experimental data. It has been necessary to design a DAQ system for data collecting and the estimation of the machine parameters. A simple user graphic interface for estimation of machine parameter has also been designed. Experimental results have validated the trend shown in Simulation results regarding evolution of the frequencies associated to faults and magnitudes of machine signatures such as amplitude of currents, torque and speed for different operation points of the motor. However, it has been observed a strong dependence between the magnitude of these frequencies and the machine signatures with the parameters.

Fault diagnosis of induction motors has been another of the objectives. The work carried out in this field has been published in international conferences and journals. Despite the fact that models only account main MMFs, results proved the suitability of them for this purpose.

Summarizing, models presented allow the user to carry out a qualitative analysis of electrical and mechanical faults on IMs based on main MMFs offering an accurate representation of the main fault effects over the currents suitable for drives applications.

References - selected positions

- [1]. G.B. Kliman, J. Stein, R.D. Endicott, R.A. Koegl, “Noninvasive Detection of Broken Rotor Bars in Operating Induction Motor”, Energy Conversion, IEEE Transactions on, vol. 3, no 4, pp. 873-879, 1988.
- [2]. T. J. Sobczyk, P. Drozdowski, “Inductances of electrical machine winding with a non-uniform air-gap”, Archiv fur Elektrotechnik, vol. 76, pp. 213-218, 1993.
- [3]. T. J. Sobczyk, P. Vas, C. Tassoni, “Models for Induction motors with air-gap asymmetry for diagnosis purposes”, ICEM Proceedings International Conference on Electrical Machines, vol. II, pp. 79-78, 1996.
- [4]. T. J. Sobczyk, K. Weinreb, T. Wegiel, M. Sulowicz, “Theoretical study of effects due to rotor eccentricities in induction motors”, In IEEE International Symposium on Diagnostics for Electrical Machines, Power Electronics and Drives (SDEMPED'99), pp.289 -295, 1999.
- [5]. T.J. Sobczyk, W. Maciołek, “Effects due to higher space harmonics in induction motor with faulty cage”, Archives of Electrical Engineering, PWN, Warsaw, vol. 51, pp. 203-215, 2002.
- [6]. S. Nandi, R.M. Bharadwaj, H.A. Toliyat, “Mixed eccentricity in three phase induction machines: analysis, simulation and experiments”, Industry Applications Conference, 2002. 37th IAS Annual Meeting. Conference Record of the, vol.3, pp. 1525-1532, 2002.
- [7]. B. Ozpineci, L. M. Tolbert, “Simulink implementation of induction machine model - a modular approach”, IEMDC 2003 In Electric Machines and Drives Conference, vol. 2, pp. 728-734, 2003.

Summary “Simulink models of faulty induction machines for drives applications”

- [8]. J. Faiz, I. T. Ardekanej, H. A. Toliyat, “An evaluation of inductances of a squirrel-cage induction motor under mixed eccentric conditions”, *Energy Conversion, IEEE Transactions on*, vol. 18, no. 2, pp. 252-258, 2003.
- [9]. T.J. Sobczyk, W. Maciołek, “Does the component $(1-2s)$ fo in stator currents is sufficient for detection of rotor cage faults?”, *Proc. 5th IEEE Symp. on Diagnostics of Electric Machines, Power Electronics and Drives, (SDEMPED 2005)*, pp. 175-179, 2005.
- [10]. A. Siddique, G.S. Yadava, B. Singh, “A review of stator fault monitoring techniques of induction motors”, *Energy conversion, IEEE transactions on*, vol. 20, no. 1, pp. 106-114, 2005.
- [11]. G. M. Joksimović, “Dynamic simulation of cage induction machine with air gap eccentricity”, *IEE Proceedings-Electric Power Applications*, vol. 152, no. 4, pp. 803-811, 2005.
- [12]. A. Bellini, C. Concari, G. Franceschini, E. Lorenzani, C. Tassoni, A. Toscani, “Thorough understanding and experimental validation of current sideband components in induction machines rotor monitoring”, *IEEE Industrial Electronics, IECON 2006 - 32nd Annual Conference on*, pp. 4957-4962, 2006.
- [13]. A. A. Ansari, D. M. Deshpande, “Mathematical Model of Asynchronous Machine in MATLAB Simulink”, *International Journal of Engineering Science and Technology*, vol. 2, no. 5, pp. 1260-1267, 2010.
- [14]. A. Aktaibi, D. Ghanim, “Dynamic simulation of a three phase induction motor using Matlab Simulink”, 2011.
- [15]. C. Kreischer, L. Golebiowski, “Comparison of different methods to determine defects in the stator core”, *Electrical Machines (ICEM), 2012 XXth International Conference on*, pp. 1608-1611, 2012.
- [16]. J. Martinez, A. Belahcen, A. Arkkio, “Broken bar indicators for cage induction motors and their relationship with the number of consecutive broken bars”, *IET Electric Power Applications*, vol. 7, no. 8, pp. 633-642, 2013.
- [17]. W. L. Leedy, “Simulink/MATLAB Dynamic Induction Motor Model for Use as A Teaching and Research Tool”, *International Journal of Soft Computing and Engineering (IJSCE)*, vol. 3, no. 4, pp. 102-107, 2013.
- [18]. K. Weinreb, “Diagnostics of an induction-motor rotor by the spectral analysis of stator currents”, *Thermal Engineering*, vol. 60, no. 14, pp. 1006-1023, 2013.
- [19]. J. Anju, V. Jose, D. Sebastian, “Stator fault detection in induction motor under unbalanced supply voltage”, *Emerging Research Areas: Magnetics, Machines and Drives (AICERA/iCMMMD), 2014 Annual International Conference on*, pp. 1-6, 2014.

Books

- [1]. G. M. Fichtenholz, “Differential and integral calculus”, tom. 3, Warsaw: PWN (in Polish), 1980.
- [2]. P. Vas, “Sensorless Vector and Direct Torque Control”, Oxford: Oxford Science Publications, 1998.
- [3]. J. Fraile Mora, “Electrical Machines”, edn.VI. Madrid: McGraw-Hill, 2003.
- [4]. T.J. Sobczyk, “Methodological aspects of mathematical modelling of induction machines” (in Polish), WNT, Warsaw, 2004.
- [5]. I. Boldea, “The induction machines design handbook”, CRC press, 2009.
- [6]. A. D. Poularikas, “Handbook of formulas and tables for signal processing”, CRC Press, 2010.

Summary “Simulink models of faulty induction machines for drives applications”

- [7]. P. Waide, C. U. Brunner “Energy-Efficiency Policy Opportunities for Electric Motor-Driven Systems”, IEA - International Energy Agency, Energy Efficiency Series, 2011.
- [8]. Krause, Paul C, Wasynczuk O., Sudhoff S. D, Pekarek S., “Analysis of electric machinery and drive systems”, John Wiley & Sons, 2013.

Publications issued by the author in conferences

- [1]. A.J. Fernandez Gomez, T.J. Sobczyk, “Comparison of Fourier spectra of induction machine for cage asymmetry and faults in mechanical part of a drive”, CM 2013 and MFPT 2013, 2013.
- [2]. A. J. Fernandez Gomez, T. J. Sobczyk, “Motor current signature analysis apply for external mechanical fault and cage asymmetry in induction motors”, Diagnostics for Electric Machines, Power Electronics and Drives (SDEMPED), 2013 9th IEEE International Symposium on, pp. 136-141, 2013, (IEEE Xplore Digital Library).
- [3]. A. J. Fernandez Gomez, A. Dziechciarz, T.J. Sobczyk, “Mathematical modeling of eccentricities in induction machines by the mono-harmonic model”, Diagnostics for Electric Machines, Power Electronics and Drives (SDEMPED), 2013 9th IEEE International Symposium on, pp. 317-322, 2013, (IEEE Xplore Digital Library).
- [4]. A. J. Fernandez Gomez, “Simulink models of faulty induction machines for drivers applications”, International PhD Workshop OWD13, conference archives PTETiS, vol. 33, pp. 204-209, 2013.
- [5]. A. J. Fernandez Gomez, Victor H. Jaramillo, James R. Ottewill, “Fault detection in electric motors by means of the extended Kalman Filter as disturbance estimator”, Control (CONTROL), 2014 UKACC International Conference on, pp. 432 - 437, 2014, (IEEE Xplore Digital Library).
- [6]. A. J. Fernandez Gomez, T.J. Sobczyk, K. Weinreb, “Influence on Rotor Broken Bar Faults Diagnosis of Mechanical Torque Pulsations by Means of FFT”, Diagnostics for Electric Machines, Power Electronics and Drives (SDEMPED), 2015 10th IEEE International Symposium on (Submitted), 2015.

Publications issued by the author in Journals

- [1]. A.J. Fernandez Gomez, T.J. Sobczyk, “Influence of design data of induction motor on effects of cage asymmetry”, Prace Naukowe Instytutu Maszyn, Napędów I Pomiarów Elektrycznych Politechniki Wrocławskiej, Vol. I, pp 357-364, 2012.
- [2]. A. J. Fernandez Gomez, T.J. Sobczyk, “Influence of Induction Motor Design Data on Effects of Cage Asymmetry”, Journal of Energy and Power Engineering, vol. 7, no. 8, pp 1586-1591, 2013.
- [3]. A. J. Fernandez Gomez, M. Sułowicz, T.J. Sobczyk, “Induction motor signatures analysis under influence of mechanical and electrical fault”, Instytut Napędów I Maszyn Elektrycznych KOMEL, vol. 104, pp 293-300, 2014.
- [4]. A. J. Fernandez Gomez, M. Sułowicz, T.J. Sobczyk, “Influence of mechanical faults on induction machines with electrical faults”, Czasopismo Techniczne Elektrotechnika, 2015.